Structure, Vol. 12, 1245–1255, July, 2004, ©2004 Elsevier Ltd. All rights reserved. DOI 10.1016/j.str.2004.04.018

Pathway Complexity of Alzheimer's β-Amyloid $A\beta_{16-22}$ Peptide Assembly

Sébastien Santini,[1] Guanghong Wei,[2] Normand Mousseau,[2] and Philippe Derreumaux[3,*]

[1]Information Génomique et Structurale
CNRS UPR 2589
31 Chemin Joseph Aiguier
13402 Marseille Cedex 20
France

[2]Département de Physique and Regroupement Québécois sur les Matériaux de Pointe
Université de Montréal
C.P. 6128
Succursale Centre-ville, Montréal, Québec
Canada

[3]Laboratoire de Biochimie Théorique
UPR 9080 CNRS
Institut de Biologie Physico-Chimique and
Université Paris
13 rue Pierre et Marie Curie
75005 Paris
France

Summary

Recent studies suggest that both soluble oligomers and insoluble fibrils have toxic effects in cell cultures, raising the interest in determining the first steps of the assembly process. We have determined the aggregation mechanisms of $A\beta_{16-22}$ dimer using the activation-relaxation technique and an approximate free energy model. Consistent with the NMR solid-state analysis, the dimer is predicted to prefer an antiparallel β sheet structure with the expected registry of intermolecular hydrogen bonds. The simulations, however, locate three other antiparallel minima with nonnative β sheet registries and one parallel β sheet structure, slightly destabilized with respect to the ground state. This result is significant because it can explain the observed dependency of β sheet registry on pH conditions. We also find that assembly of $A\beta_{16-22}$ into dimers follows multiple routes, but α-helical intermediates are not obligatory. This indicates that destabilization of α-helical intermediates is unlikely to abolish oligomerization of Aβ peptides.

Introduction

Past studies of the role of the amyloid β-protein (Aβ) in Alzheimer's disease have linked the neurotoxicity of Aβ with its tendency to form amyloid fibrils (Selkoe, 1998). However, accumulating evidence suggests some of the important toxic species of Aβ are soluble Aβ oligomers (early aggregates) (Walsh et al., 2002). This finding supports an important role for Aβ oligomers in the etiology of Alzheimer's disease and thus make Aβ oligomers attractive therapeutic targets (Wolfe, 2002). If effective drug design strategies targeting Aβ oligomers are to be developed, it is essential to obtain a detailed knowledge of the structures and assembly dynamics of these oligomers.

A detailed experimental characterization of these oligomeric intermediates is thus far very difficult, and only limited data are available because the intermediates are typically short lived and are present in a wide range of conformations and degrees of aggregation. We know, however, that these oligomers tend to be small. Using photo-induced cross-linker, the oligomer size distributions of aggregate-free, low molecular weight (LMW) $A\beta_{1-40}$ and $A\beta_{1-42}$ could be assessed quantitatively (Bitan et al., 2003). This experimental study revealed that LMW $A\beta_{1-40}$ is a mixture of monomers, dimers, trimers, and tetramers, in rapid equilibrium, while LMW $A\beta_{1-42}$ tends to exist in larger pentamer/hexamer units. It is these structures that would self-assemble to form larger oligomers (Bitan et al., 2003). We also have some limited information on the structure of the intermediates. Studying the secondary structural changes of various $A\beta_{1-40}$ and $A\beta_{1-42}$ fragments during fibrillogenesis, Walsh et al. and Kirkitadze et al. observed the formation of an oligomeric intermediate containing 29%–32% α helix (Walsh et al., 1997, 1999; Kirkitadze et al., 2001). It was not until the α helix formation process had begun, as revealed by circular dichroism, that fibrils were detected by electron microscopy. But, there is also experimental evidence that helix stabilization may facilitate as well as inhibit fibril formation, depending on its strength (Fezoui and Teplow, 2002).

Recently, several structural models for Alzheimer's β-amyloid fibrils based on experimental constraints from solid state have been proposed. These studies showed that, in $A\beta_{10-35}$ (Benzinger et al., 2000) and $A\beta_{10-40}$ (Petkova et al., 2002) fibrils, peptides form parallel β sheet structures. In this notation $A\beta_{n-m}$ indicates residues *n* and *m* of full-length β-amyloid protein. In contrast, an antiparallel β sheet registry was found for smaller fragments such as $A\beta_{11-25}$ (Sikorski et al., 2003; Petkova et al., 2004), $A\beta_{34-42}$ (Lansbury et al., 1995), and $A\beta_{16-22}$ (Balbach et al., 2000). Because of its simplicity, $A\beta_{16-22}$ of sequence KLVFFAE is an attractive system for molecular modeling studies. Furthermore, $A\beta_{16-22}$ comprises the central hydrophobic core that is thought to be important in full-length Aβ assembly and contains four occurring Alzheimer's disease-causing mutations. They have been termed Flemish (A21G), Dutch (E22Q), Italian (E22K), and Artic (E22G) (Miravalle et al., 2000). $A\beta_{16-22}$ has also been investigated by molecular dynamics (MD) simulations with explicit solvent. Ma and Nussinov studied the stability of octamer of $A\beta_{16-22}$ packed in different arrangements by MD at 330 K in explicit solvent (Ma and Nussinov, 2002). They concluded that the antiparallel β sheet/parallel layer model (each layer consisting of four β strands) is the most stable, but other supramolecular structures may be correct. Although these simulations are important in understanding the supramolecular organization of the fibrils, they do not provide any information on

*Correspondence: philippe.derreumaux@ibpc.fr

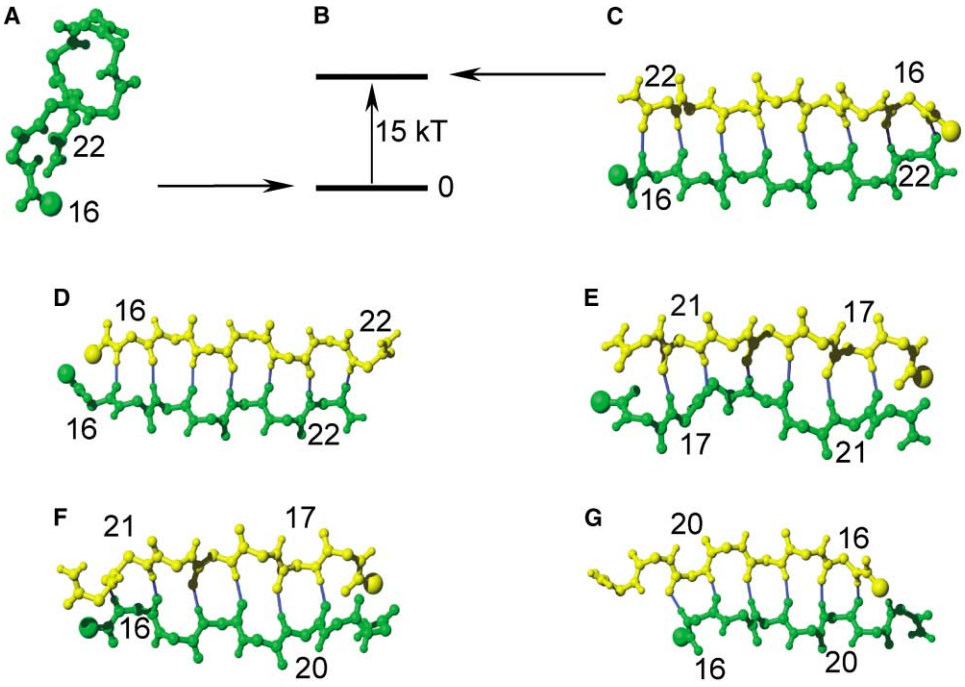

Figure 1. Lowest Energy Structures of $A\beta_{16-22}$ in Monomeric and Dimeric Forms as Predicted by ART Simulations

(A) Native state of the monomer.

(B) Energy difference between the ground state of the monomer and its conformation within the dimeric optimized form.

(C) Ground state of the dimer, antiparallel in character and described by the 16 + k ↔ 22 − k β sheet registry. (D) Parallel β sheet structure. (E–G) The three other antiparallel β sheet organisations: pattern II (E), pattern III (F), and pattern IV (G). In all figures, the N-terminal end in each chain is located by a sphere.

the oligomerization process of the peptides. Klimov and Thirumalai studied the folding of a trimer of $A\beta_{16-22}$ by MD at 300 K using an all-atom model of the protein, an explicit solvent model and a bias to facilitate interactions between the peptides (Klimov and Thirumalai, 2003). They found that the assembly of $A\beta_{16-22}$ trimer occurs by multiple pathways with the formation of an obligatory α-helical intermediate.

Because rapid equilibrium between monomers, dimers, and larger units has been found for $A\beta_{1-40}$ (Bitan et al., 2003) and blocking the formation of dimers could inhibit fibril formation, we have attempted recently to understand the folding mechanisms of $A\beta_{16-22}$ dimer using the activation relaxation technique (ART) (Barkema and Mousseau, 1996; Mousseau et al., 2001) coupled with OPEP, which provides for a detailed protein and unbiased energy model (Derreumaux, 1999, 2000; Forcellino and Derreumaux, 2001). These models are at variance with previous on-lattice studies (Istrail et al., 1999; Broglia et al., 1998) and off-lattice studies using low-resolution models and Go-type potentials (Ding et al., 2002; Jang et al., 2004) aimed at understanding aggregation in proteins. Preliminary results were presented in a short communication (Santini et al., 2003). Here, we offer a detailed description of the aggregation mechanisms starting from parallel β sheets. Furthermore, we present the results of new ART simulations starting from antiparallel α helices and the results of MD simulations.

These simulations show that even though the in-register antiparallel β sheet structure is the most stable structure for the $A\beta_{16-22}$ dimer, several hydrogen-bond patterns in both parallel and antiparallel orientations can exist. From the generated trajectories, we can also identify multiple folding pathways which demonstrate, in particular, that α-helical intermediates are not obligatory.

Results and Discussion

$A\beta_{16-22}$ Monomer Is Random Coil in Solution

The solution structure of $A\beta_{16-22}$ remains to be determined, but the structure of various peptides spanning this fragment has been characterized experimentally. Monomeric forms of $A\beta_{10-35}$ (Zhang et al., 2000), $A\beta_{1-40}$, and $A\beta_{1-42}$ (Zagorski et al., 2000) are essentially unstructured in aqueous solution at neutral pH, while $A\beta_{1-28}$ (Talafous et al., 1994), $A\beta_{1-40}$, and $A\beta_{1-42}$ (Shao et al., 1999) adopt a predominantly α-helical conformation in a membrane-like environment. Massy et al. found that the region 16–22 is essentially random coil (RC) in 4 ns MD simulations of the wild-type and Dutch mutant forms of $A\beta_{10-35}$ in aqueous solution (Massi et al., 2002). Klimov and Thirumalai found that the time-averaged populations of (RC, β strand, and α helix) residues in $A\beta_{16-22}$ monomers are (56%, 33%, and 11%) using 8 ns MD trajectories and their specific definitions for assigning conformational states to the residues (Klimov and Thirumalai, 2003). From our ART-generated trajectories we find that the populations of (RC, β strand, and α helix) residues are (77%, 18%, and 5%) using Klimov's defini-

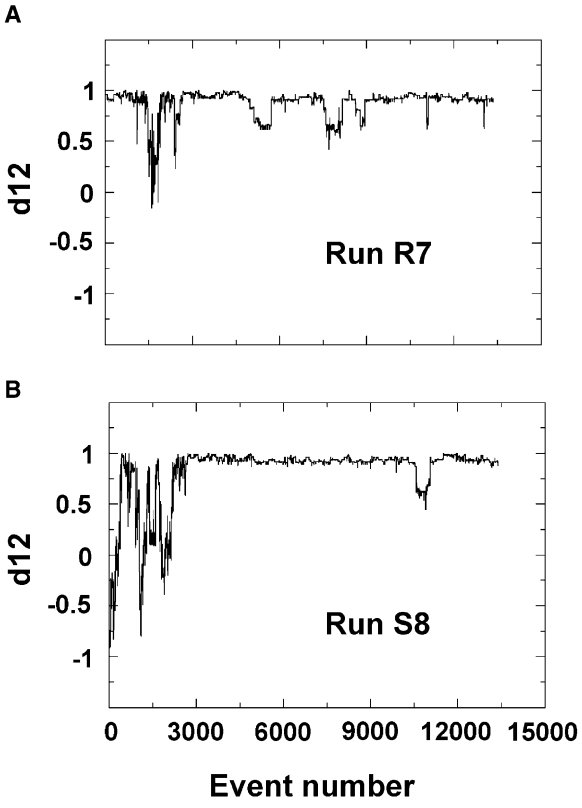

Figure 2. Orientation of the Peptides

Variations of the orientation of the chains (d12) as a function of accepted events in the ART runs R7 (A) and S8 (B).

tions and (96%, 2%, and 2%) using DSSP. The lowest energy structure, compact, and random coil, generated by all ART simulations is shown in Figure 1A. The energy spectrum of the calculated conformational states in Figure 1B shows that the conformation of $A\beta_{16-22}$ monomer within the dimeric optimized form (Figure 1C) is destabilized by 9 kcal/mol (15 kT) with respect to its native compact state. Our model is therefore consistent with the conformational change of Aβ and prion proteins observed upon association.

$A\beta_{16-22}$ Can Adopt Different Hydrogen Bond β Sheet Registries

ART search using OPEP indicates that the global energy minimum of the dimer matches exactly the solid-state NMR model proposed by Balbach et al. at pH 7.4, namely the pattern of H bonds depicted between layer II (middle) and layer III (bottom) in figure 10 of (Balbach et al., 2000). This conformation, obtained starting from antiparallel α helices (event 5,759 in run S1) or parallel β sheets (events 10,853 in R1, 2,594 in R6, and 6,467 in R9), is characterized by the 16 + k ↔ 22 − k β sheet registry and an energy of −44.4 kcal/mol (Figure 1C). This pattern of H bonds will be referred to as pattern I. A partially folded pattern I of energy −43.3 kcal/mol is obtained in run R4 because the residues A21 and E22 are disordered in both chains.

Surprisingly, the lowest energy structures generated

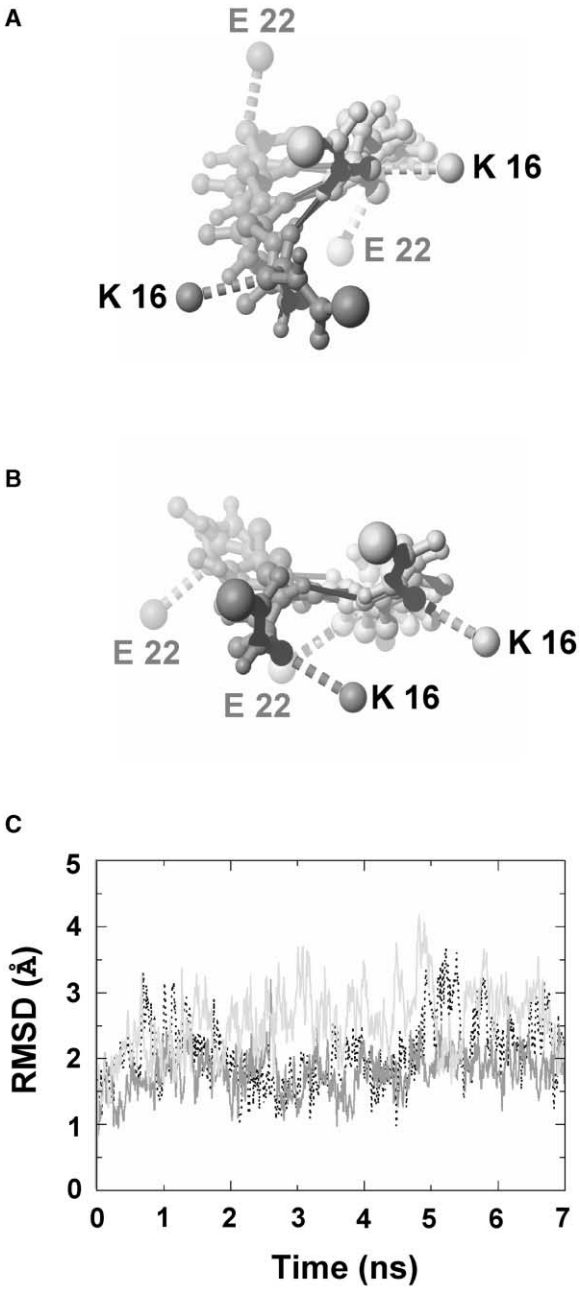

Figure 3. Comparison of the Parallel β Sheet Structures

(A) Our ART-predicted structure with the charged residues pointing to opposite directions above the plane formed by the sheets.

(B) The parallel β sheet structure, as discussed in Balbach (Balbach et al., 2000), with the K (and E) of both chains in close proximity.

(C) Rms deviations (in angstroms) of pattern I (dashed), our parallel (dark gray), and Balbach's (light gray) models from their minimized structures by 7 ns MD simulations at 330 K. The time-averaged percentage of H bond formed is 79% (pattern I), 82% (our parallel model), and 75% (Balbach's model). Identical rms deviations and percentages of H bonds are obtained for the patterns II, III, and IV (data not shown).

by the remaining 16 simulations can be clustered into four distinct β sheets (Figures 1D–1G). Three β sheets are antiparallel. They are characterized by the 17 +

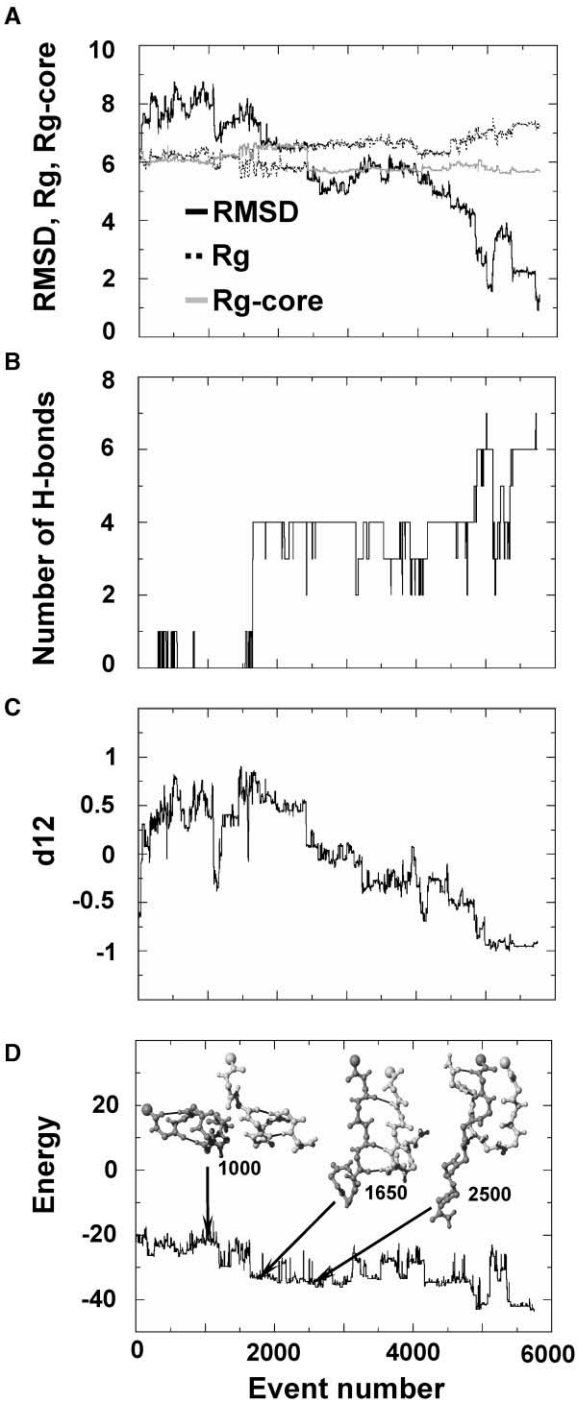

Figure 4. Variation of Order Parameters in the Folding ART Simulation S1 Leading to Pattern I

(A) Rms deviation from the ground state, Rg, and Rg-core, in angstroms; (B) number of native H bonds; (C) d12, and (D) energy in kcal/mol. The structures at events 1000, 1650, and 2500 are shown. For clarity, the results are given until the ground state is located at event 5759. Only accepted events are shown.

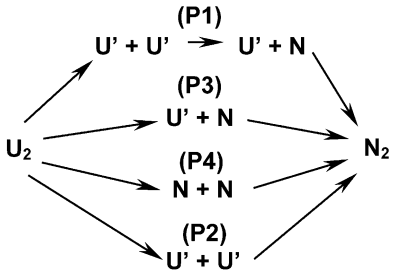

Figure 5. Four Aggregation Routes, P1–P4, Leading to the Native Assembly of the Dimer, N2

The symbols U′ and N refer to the unfolded and native states of either chains. A chain is considered native during folding if it deviates by less than 2.0 Å from its conformation in the dimeric optimized form.

k ↔ 21 − k β sheet registry (pattern II, energy of −43.4 kcal/mol, Figure 1E, found at events 11,546 in run R3 and 7,484 in run S4, this H bond network follows exactly the second derived NMR pattern depicted between layers I [top] and II [middle] in figure 10 of [Balbach et al., 2000]); or they can be described by 16 + k ↔ 21 − k (pattern III, energy of −42.4 kcal/mol, runs R2, R10, S5, and S7, Figure 1F) and 16 + k ↔ 20 − k (pattern IV, energy of −40.4 kcal/mol, run S3, Figure 1G).

In contrast, the fourth β sheet is parallel and characterized by the 16 + k ↔ 16 + k β sheet registry (Figure 1D). This conformation, of energy −41.4 kcal/mol, is explored many times, independently of the starting structure. We find that in runs R5, R7, R8, and R11, the chains easily escape from this state, but rarely explore antiparallel β sheets; in runs S2, S6, and S8, the chains pass from antiparallel α helices to parallel β sheets permanently or quasi-permanently (see Figure 2 for runs R7 and S8) over the length of our simulations. We know, however, that these runs would eventually reach the pattern I if they were continued (Wei et al., 2003). Our parallel β sheet structure differs from that considered by Balbach et al. (Balbach et al., 2000) in two respects. Our model contains seven H bonds versus six H bonds in Balbach's model. This is to be compared with eight H bonds within pattern I and six H bonds within patterns II, III, and IV. Furthermore, the charged residues Lys16 and Glu22 are on opposite sides of the β sheet in our model and not in close proximity as in Balbach's model (Figures 3A–3B). All these models are stable in MD simulations with water at 330 K, independently of the initial velocities. In Figure 3C, we have selected to plot the C_α rms deviation of three models from their mimimized energy structures as a function of time. We see that the Balbach's model is less rigid than our parallel structure and the pattern I, but all models are very stable within the 7 ns timescale. We recognize that the degree of MD sampling presented here is not sufficient to assess the stability of the models and that other fields can modify the results. However, the results do not change when extending the simulation of pattern I from 7 to 20 ns (data not shown), i.e., on a timescale feasible using current computer facilities, and the GROMOS force field has been extensively tested against experimental data (Berendsen et al., 1995).

Taken together, our results suggest that several hydrogen bond β sheet registries of similar energy are available for the $A\beta_{16-22}$ dimer. This finding complements recent MD simulations of a trimer of the heptapeptide

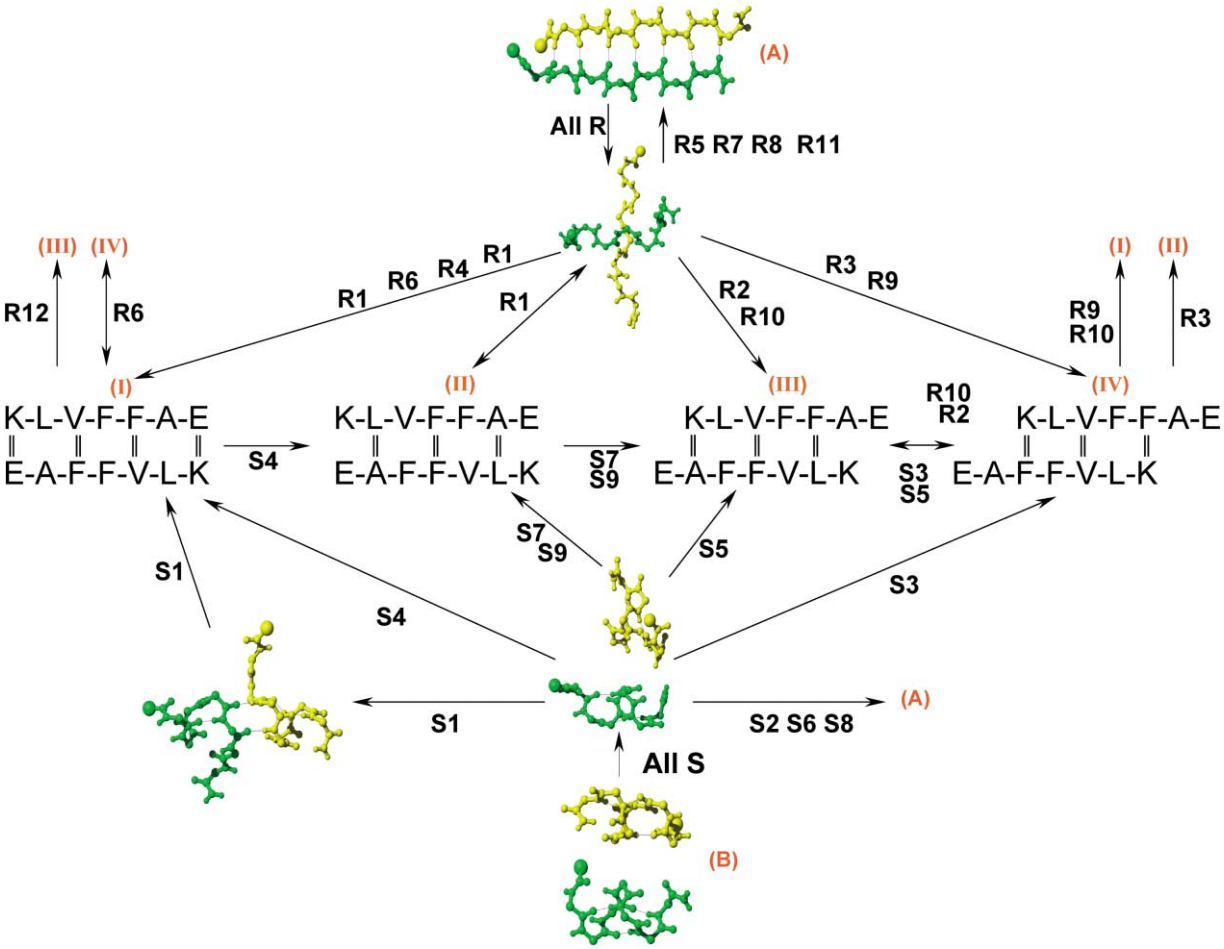

Figure 6. Detailed Aggregation Motions Leading to the Patterns I–IV

All the ART simulations starting from the parallel β structure (A) are denoted by R and pass through a perpendicular state. All the ART simulations starting from the two parallel α helices (B) are denoted by S. One-way transition observed in our simulations is represented by a single arrow, two-way transition by a double arrow. H bonds are represented by vertical double bars.

GNNQQNY from the yeast prion Sup35 which point to three minima associated with parallel, antiparallel, and mixed parallel-antiparallel β sheet structures (Gsponer et al., 2003).

Atomic Assembly Trajectories

Among a total of 21 runs, 8 runs from parallel β sheets (R1–R4, R6, R9, R10, and R12), and 6 runs from antiparallel α helices (S1, S3–S5, S7, and S9) locate antiparallel β sheet structures of very low energy within the allotted number of events. In what follows, the other runs, which essentially sample parallel β sheets, are left out of the discussion.

Table 1. Detailed Mechanisms between the Four Observed Antiparallel β Sheet Registries

Transition	Motion	Simulation
I → II	Rot2	S4, R1
I → III	Rot1 + Rep1	R12
I → IV	Rep2	R6, R9, R10, S1, S3, S5
II → III	Rot1 + Rep1	S7, S9
II → IV	Rot2 + Rep2	ND
III → IV	Rot1 + Rep1	S3, S5, R2, R10

Rot1: rotation of one chain. This always comes with a reptation by 1 residue. Rot2: rotation of both chains. RepX: reptation of one strand by X residues.

The folding trajectory R1 was described in atomistic detail elsewhere (Santini et al., 2003). We have shown that both chains rapidly loose their nonnative H bonds, then rotate in respect to one another through a perpendicular registry with one chain partially unfolded and the other fully extended, and finally adopt the antiparallel pattern I by progressive zipping of the H bonds. Here, we select to describe first the folding simulation S1 starting from two antiparallel α helices and then the general routes by which the two chains assembly to their lowest energy states.

Figure 4 shows the variation of several order parameters in the folding simulation S1. During the first 1000 events, both chains remain helical but progressively rotate in respect to one another (Figure 4C). Then the chains, parallel in character, unfold and adopt U-like conformations (see event 1650 in Figure 4C). In this first

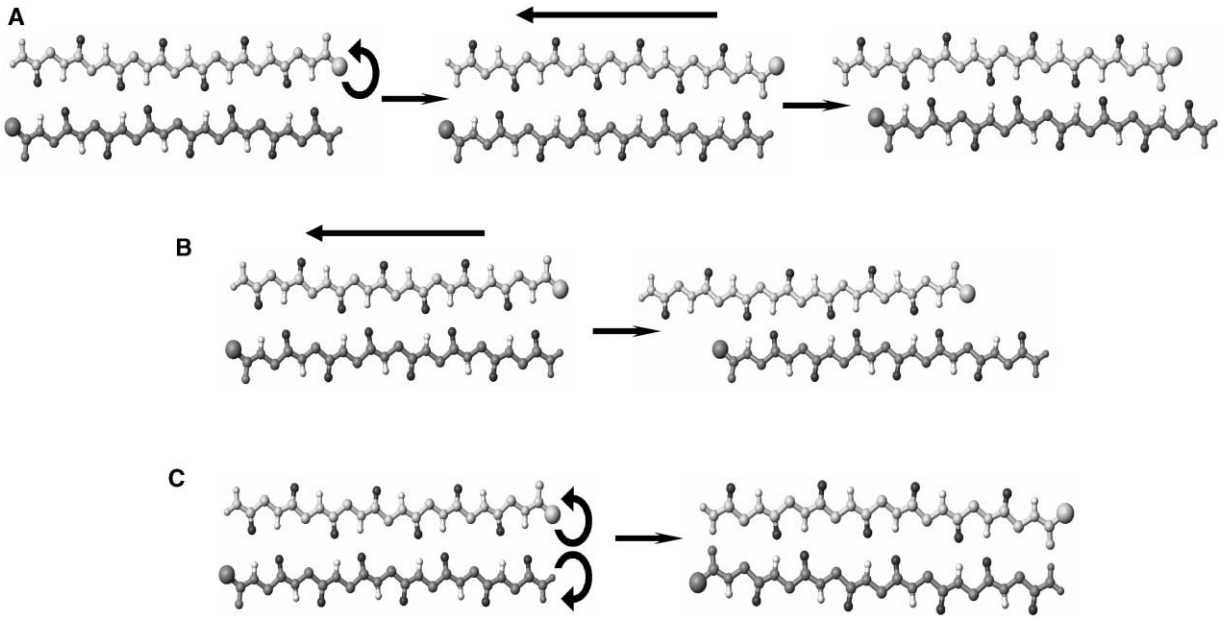

Figure 7. Schematic Representations of the ART-Generated Mechanisms between the Antiparallel Patterns

Patterns I and III (run R12), patterns II and III (runs S7 and S9), and patterns III and IV (runs R2, R10, S3, and S5) can exchange through the rotation of one chain, followed by the reptation of one strand by one residue. The I → III transition is represented in (A). A reptation move of one strand by two residues allows the chains to exchange patterns I and IV (runs R6, R9, R10, S1, S3, and S5). The I → IV transition is represented in (B). Patterns I and II (run S4) interchange by rotating both chains (C).

phase, the rms deviation with respect to the ground state, Rg, and Rg-core do not vary much (Figure 4A). At event 1700, four native H bonds form (Figure 4B). From this core of H bonds, one chain extends, whereas the other remains U-like (see cooperative decrease in rmsd and Rg-core and increase in Rg around event 2500). The conformation at event 2500, shown in Figure 4C, is characterized by the N-terminal of chain 1 and the C-terminal of chain 2 antiparallel, but the N-terminal of both chains parallel. From there, the chains find a way to locate the ground state at event 5759. It is interesting to note that the structure at event 2500 is explored, independently of the starting conformation. It is encountered (within 1.0 Å rms deviation) in runs R1 and S4.

By following the rms deviation of each chain with respect to its conformation within the dimeric optimized form for each individual folding trajectory, we find that there are four routes leading to the antiparallel β sheets (Figure 5). In pathway I, both chains unfold (U′); then, one of the chains adopts its native state (N), whereas the other remains unfolded (U′); subsequently, the native assembly occurs (N2). In pathway II, the native assembly of the dimer occurs directly from both chains unfolded, whereas in pathway III it occurs from one chain in its native state and the other unfolded. Finally, in pathway IV, native assembly occurs from both chains in their native states. All these routes are not equiprobable. Pathway I is observed in 7/14 of the runs (R1, R2, R4, S1, S3, S5, and S9), pathway III in 4/14 (R3, R10, S4, and S7), pathway IV in 2/14 (R6 and R9), and pathway II in 1/14 (R12). Overall, our simulations are consistent with previous Monte Carlo simulations using on-lattice protein models (Dima and Thirumalai, 2002; Harrison et al., 2001). Our preferred pathway for assembly occurring directly from one of the chains folded agrees with the general concept that protein aggregation arises from partially folded intermediates (Kelly, 1996; Chiti et al., 1999). On the other hand, assembly from random coils (pathway II) is supported by experimental studies on the two-state U1A and CI2 folders (Silow et al., 1999) and myoglobin (Fandrich et al., 2003).

H Bonds Provide Evidence for Very Complex Aggregation Routes

An important aspect that emerges from our simulations is that folding proceeds through multiple very complex routes as indicated by the various networks of H bonds explored. Figure 6 summarizes all the folding routes starting from parallel β sheets or antiparallel α helices. Consistent with the solid-state NMR analysis, the patterns I and II of H bonds are highly populated, but the patterns III and IV have to be taken into account. Interestingly, none of these patterns represent a dead end in our simulations. For instance, in run S4, the dimer explores transient conformations of pattern I-type before reaching the pattern II; in run R9, the dimer samples the pattern IV before reaching the pattern I; in run S4, the dimer momentarily explores the pattern I and then switches to the pattern II. The molecular mechanisms propagating the conformational changes between the various patterns of H bonds are listed in Table 1 and are described in atomistic detail in Figure 7. These conformational changes can involve a rotation of one chain (Rot1) or both chains (Rot2) by 180° around their strand axes, a reptation move (Wei et al., 2003) of one strand of the β sheet with respect to the other (RepX where X

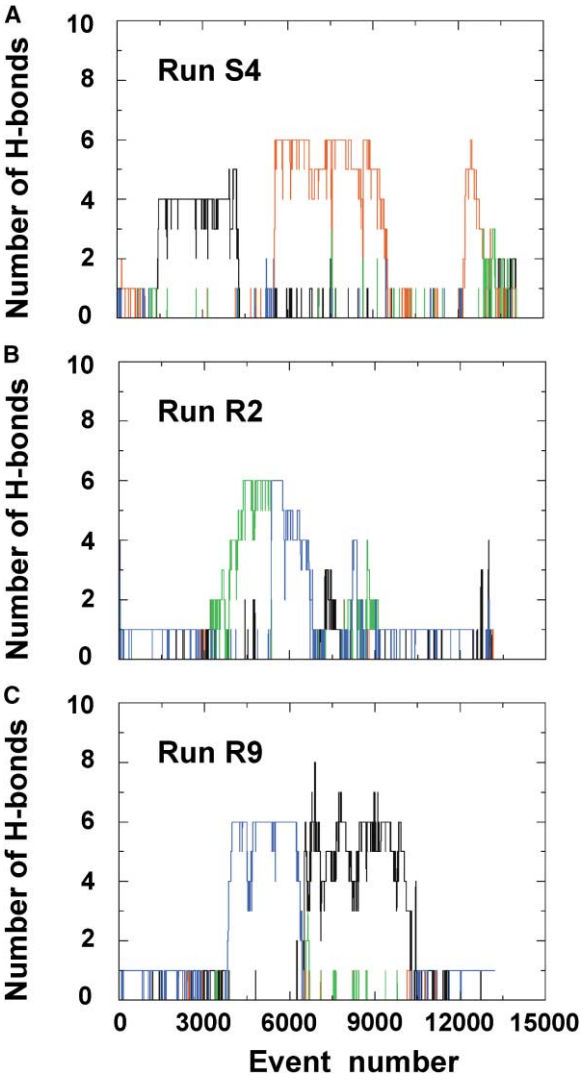

Figure 8. Evolution of H Bonds

Number of H bonds satisfying patterns I–IV in ART runs S4 (A), R2 (B), and R9 (C) as a function of accepted event numbers. Pattern I, black; pattern II, red; pattern III, green; and pattern IV, blue.

represents the number of residues shifted) or a combination of these two mechanisms. Specifically, we find that the dimer can exchange the patterns I and II (runs R1 and S4) by a Rot2 mechanism (Figure 7C). Transitions between the patterns I and III (run R12), the patterns II and III (runs S7 and S9), and the patterns III and IV (runs R2, R10, S3, and S5) occur by a combined Rot1+Rep1 mechanism (Figure 7A). Finally, the Rep2 mechanism, which allows the exchange between the patterns II and IV (Figure 7B) and does not need rotation of the chains, is easily explored. It is encountered in runs R6, R9, R10, S1, S3, and S5. We note that the transition between the patterns II and IV by a combined Rot2+Rep2 mechanism is not observed in this study, but this could not be totally excluded if we had run 100 runs.

The transitions between the patterns can be fast or slow. Figure 8 shows the number of H bonds satisfying each pattern as a function of accepted events in the runs R2, R9, and S4. We see that the exchange between the patterns III and IV takes 34 events in run R2 (Figure 8B) but 1052 events in run R10. The patterns I and II interchange within 1350 events in run S4 (Figure 8A) versus 7100 events in run R1. The change between the patterns IV and I takes 620 and 800 events in runs R9 (Figure 8C) and R6, respectively. The barrier height to go from one pattern to another without any bias (defined here by the difference between the highest energy minimum and the energy of one pattern during the transition) is ~20 kcal/mol, independently of the patterns involved. We recognize that these energy barriers likely are much smaller using the all-atom model and explicit solvent as discussed in Experimental Procedures.

Nonhelical Conformations Are Possible Intermediates

Using circular dichroism and electron microscopy, Kirkitadze et al. (Kirkitadze et al., 2001) and Walsh and coworkers (Walsh et al., 1997, 1999) have identified an α helix-containing intermediate prior to the formation of β sheet-rich assembly of $A\beta_{1-40}$, $A\beta_{1-42}$, and several variants. Based on MD simulations of $A\beta_{16-22}$ trimer at 300 K, Klimov and Thirumalai have proposed recently that the antiparallel β sheet could occur by multiple pathways with the formation of an obligatory α-helical intermediate (Klimov and Thirumalai, 2003). But another interpretation is also possible: for instance, a mechanism involving rapid equilibrium between these α-rich oligomers incapable of maturing into fibrils and smaller Aβ oligomers or Aβ monomers which could form fibrils through an alternative pathway (Kirkitadze et al., 2001).

In order to detect whether α helix conformations occur prior to optimal assembly of the sheets, we have followed the secondary structure composition of the chains as a function of events using both Klimov's definitions and the DSSP program (Figure 9). Our 14 (8 R + 6 S) folding simulations clearly show that the occurrence of a helical intermediate is not an obligatory step for $A\beta_{16-22}$ dimer using the DSSP program. Starting from parallel β sheets, intermediates containing 30% helix are observed in runs R1, R2, R4, R10, and R12, but not in runs R3, R6, and R9. On the other hand, starting from antiparallel α helices, helical intermediates are detected in runs S1, S3, S5, S7, and S9, but not in S4. In the analysis starting from helices, we consider a helical intermediate if it occurs after 1000 accepted events. It is interesting to note that by using Klimov's, definitions helical intermediates are detected in R3 between events 4000 and 6000 (Figure 9B), in R6 around events 1000 (9C), and in R9, but not in S4.

Atomic analysis of the helical intermediates shows that the helix can be found in either chain with a strong preference for encompassing residues VFF. For instance, in run R1, the intermediate between events 3400 and 3660 has a α helix spanning residues LVFF in chain 2 (Figure 9A), and the intermediate between events 5,790 and 5,820 has a α helix spanning residues VFFA in chain 1. In contrast, helix spans residues VFFA in chain 2 (events 3,860 in R2; 1,441 in S1; and 2,576 in S9), residues LVFF in chain 1 (events 2,722–2,741 in run S3; event 607 in run S4), or residues VFFA in chain 1 (events

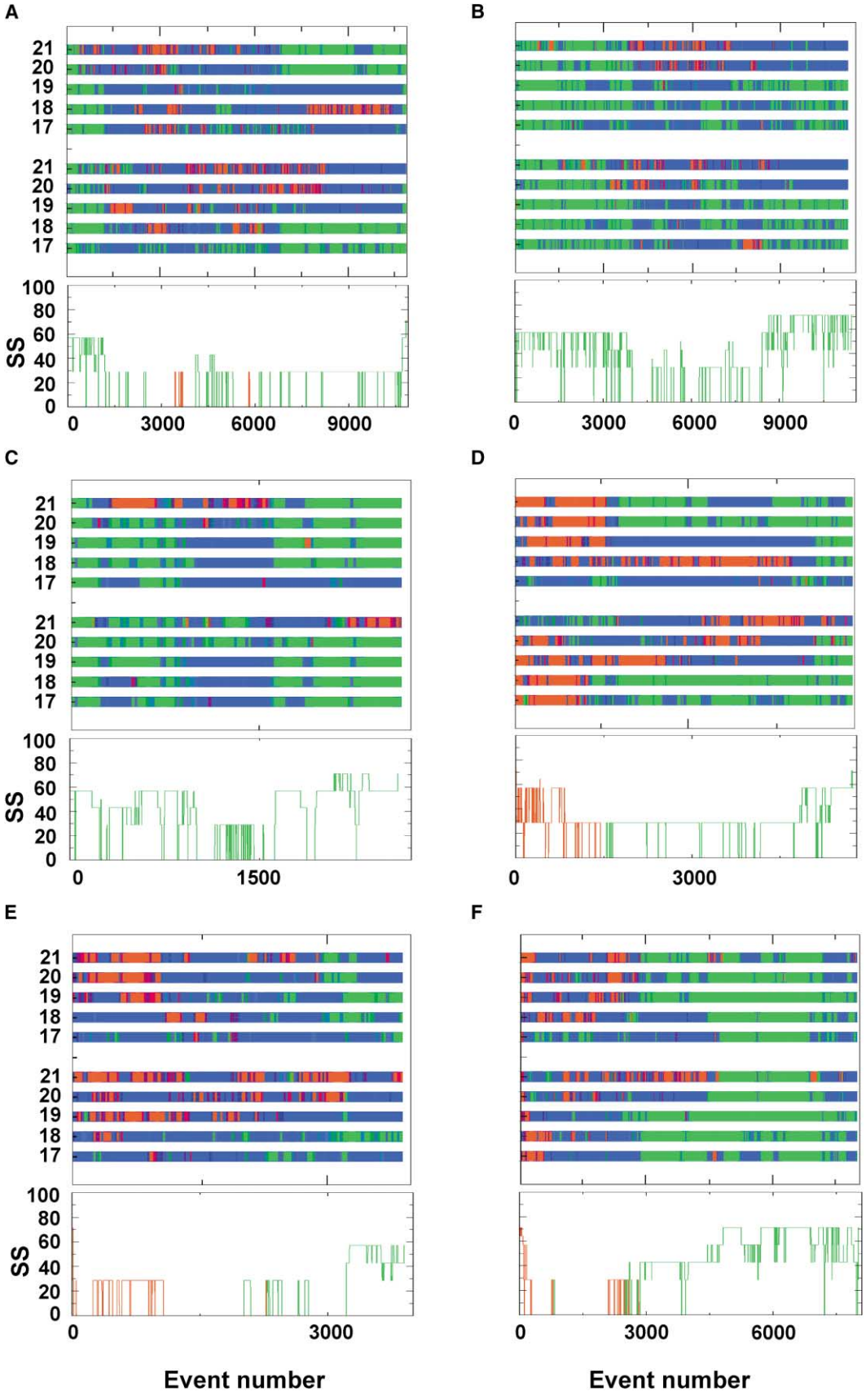
A
B
C
D
E
F
21
20
19
18
17
SS
100
80
60
40
20
0
0
3000
6000
9000
1500
Event number

6,746 in R4; 3,586 in R10; 10,099 in R12; 2,274 in S5; and 1,428 in S7). We did not find evidence of structural similarity between these intermediates, all structures deviating by more than 3.0 Å rms from each other.

Conclusions

The present study has attempted to determine the folding pathways for $A\beta_{16-22}$ assembly into a dimer. Our analysis is based on ART simulations starting from parallel β sheets and antiparallel α helices, but identical results are obtained from arbitrarily chosen conformations (data not shown). These simulations are free of any biases to facilitate interactions between the chains and use a generic energy model which was found to work well on small proteins adopting various secondary structures in their optimized monomeric forms. Additional MD simulations with an all-atom representation of the peptides are also performed to verify the stability of the ART-predicted conformations of low energy in solvent on the nanosecond timescale.

Although the structure in $A\beta_{16-22}$ fibrils from solid-state NMR at pH 7.4 (Balbach et al., 2000) depends on the intrasheet and intersheet molecular interactions, it is interesting that the lowest energy structure of the dimer in ART-OPEP simulations is antiparallel in character with the NMR 16 + k ↔ 22 − k β sheet registry. Hovever, the simulations also locate three alternative antiparallel organizations with different β sheet registries and one parallel β sheet assembly, slightly destabilized relative to the ground state. This result is significant because it helps clarify the variation of β sheet registry on pH conditions (Petkova et al., 2004) and amino acid compositions (Tjernberg et al., 2002). In addition to finding these low-energy minima, our simulations also describe the molecular mechanisms propagating these conformational changes and emphasize the crucial role of the reptation move of one strand of the β sheet with respect to the other. Again, this is consistent with very recent isotope-edited infrared spectroscopy on the protein prion fragment spanning residues 109–122, which points to the reptation move of the central strand within a trimer (Silva et al., 2003). Finally, this study makes it clear that multiple aggregation routes are possible, but α-helical conformations are not obligatory intermediates for the dimer. It is possible that a minimum Aβ length is needed—there is no available circular dichroism study for $A\beta_{16-22}$ as for $A\beta_{1-40}$ (Kirkitadze et al., 2001)—or that a minimum oligomeric size (trimeric or larger) is needed for the chains to gain stability by forming α helices. ART simulations of $A\beta_{16-22}$ in trimeric and hexameric forms are underway to address these issues and provide us with a more complete folding picture for fibril formation.

Experimental Procedures

The N and C termini of each chain were neutralized using acetyl and amine groups, respectively, as done experimentally (Balbach et al., 2000). The folding trajectories were obtained by the activation-relaxation technique (ART nouveau [Mousseau et al., 2001]) using the OPEP energy model (Derreumaux, 1999, 2000; Forcellino and Derreumaux, 2001). The all-atom MD simulations were not used to fold the two monomers, but rather to test the stability of some ART-predicted configurations in explicit solvent.

ART-OPEP Simulations

A complete description of the ART-OPEP procedure has been given elsewhere (Santini et al., 2003; Wei et al., 2002, 2003). In brief, the protein model uses a simplified chain representation with all backbone atoms included (i.e., N, H, C_α, C, and O) and all side chains modeled by a bead with an appropriate van der Waals radius and geometry. The OPEP (*o*ptimized *p*otential for *e*fficient peptide-structure *p*rediction) energy model (version 1.3) is expressed as a function of three types of interactions: terms to satisfy stereochemistry, pairwise contact potential between main chain particles, side chain-main chain and side chains (considering all 20 amino acid types), and backbone two-body and four-body hydrogen bonding interactions (Santini et al., 2003; Wei et al., 2002).

A basic ART event consists of four steps. Starting from a minimum, the system is pushed outside the harmonic well until a negative eigenvalue appears in the Hessian matrix. The system is then pushed along the eigenvector associated with the negative eigenvalue until the total force is close to zero, indicating a saddle point. The first two steps constitute the activation phase. Subsequently, the configuration is pushed slightly over the saddle point and is relaxed to a new local minimum, using standard minimization technique. Finally, the new configuration is accepted/rejected using the Metropolis criterion at the desired temperature. This four-step procedure was repeated 18,000 events for each simulation. It is important to note that since ART events bring a conformation from a fully relaxed state to another relaxed state, going through an activation barrier, the Metropolis temperature cannot be directly associated with the real temperature. In particular, ART neglects totally the vibrational contributions to the free energy of the oligomers. This constitutes one major advantage for ART: it is possible to use a higher temperature than in MD, for example, while still sampling the lowest energy conformations. Moreover, since the moves in ART simulations are defined directly in the energy landscape, the barriers crossed are defined by the problem, increasing considerably the sampling efficiency of ART with respect to MD simulations.

In this work, we have performed 21 ART simulations of the dimer using OPEP: 12 start from parallel β sheets (R1–R12) and 9 start from antiparallel α helices (S1–S9). Starting from a low-energy parallel β sheet allows us to verify that our procedure samples the configurational space appropriately. Furthermore, this organization is known to be preferred for larger Aβ fragments. The second starting point with two α helices is reminiscent of the topological change that occurs in prion proteins (Prusiner, 1997). All runs starting from the same configuration use different random-number seeds and are free of any biases to facilitate interactions between the peptides. This contrasts with the simulations reported by Klimov and Thirumalai (Klimov and Thirumalai, 2003). In most simulations, the Metropolis temperature is set to 1000 K because the parallel β sheet is only destabilized by 3 kcal/mol with respect to the antiparallel β sheet. We emphasize that at this temperature, the dimer is not stable and continues to evolve on the conformational space. Finally, three runs were also carried out on the monomer to determine its equilibrium conformations at $T_{Metropolis} = 300$ K starting from fully extended conformations.

OPEP was found recently to discriminate native from false positive conformations for a series of peptides in monomeric forms (Derreumaux, 1999, 2000; Forcellino and Derreumaux, 2001). Because OPEP is an approximate free energy model, we know that several

Figure 9. Evolution of Secondary Structure

Secondary structures as a function of accepted events during the folding ART simulations R1 (A), R3 (B), R6(C), S1(D), S5 (E), and S9 (F). They are obtained using Klimov's rules for the five inner residues (L17, V18, F19, F20, and A21) (top panel). Blue indicates random coil, green β strand, and red α helix. Or they are obtained using the DSSP program (bottom panel) and the percentages of β sheet (green) and α helix (red) are given. For clarity, the results are shown until the ground state is located.

factors can enhance the energy barriers estimated by more physically based energy functions. In particular, solvent is not treated explicitly, and hydrogen bonding interactions between the solvent and the chains certainly affect the relative energetics and entropic effects (Derreumaux and Schlick, 1998); side chains are modeled by a bead and may not capture the real complexity of hydrophobic and electrostatic interactions between side chains; the dependence of the stability of polypeptides on pH conditions is not considered. In spite of these limitations, we have found that the ART-generated pathways using OPEP are generally kinetically possible: the folding of a helix model through a transition state characterized by two α helices connected by a loop was found by ART using OPEP (Wei et al., 2002) and MD using all-atom model (Chowdhury et al., 2003). Similarly, the folding of a β hairpin model by ART identified two mechanisms described by standard protocols, but also a reptation mechanism (Wei et al., 2003) which was found recently by multicanonical simulations on another hairpin model using explicit solvent (Ikeda and Higo, 2003).

Molecular Dynamics Simulations

The MD runs used the GROMACS program and the force field GROMOS96 (Berendsen et al., 1995). The all-atom conformations discussed here were generated using the MOLMOL software (Koradi et al., 1996). The models were solvated in a dodecahedric box of 30 Å side containing $\sim$1700 SPC (simple point charge) water molecules under periodic boundary conditions. The Particle Mesh Ewald method was used with a cutoff distance of 12 Å for the van der Waals and electrostatics interactions. The models were minimized by 1000 steps of conjugate gradient and equilibrated at the desired temperature under Cα atom position restraints for 10 ps. At this stage, the restraints were released and MD simulations were performed in the canonical NPT (number of particles-pressure-temperature) ensemble at neutral pH for 7 ns. Each model was subject to two simulations using different initial velocities at 330 K, i.e., at a T often used to incubate the amyloid in experiments. The time step for dynamics was 2 fs using the SHAKE algorithm. Nonbonded interactions were updated every 20 fs. Temperature was controlled using a weak coupling to a bath of constant T (coupling time of 0.1 ps) and pressure by a weak coupling to a bath of constant P (1 atm, coupling time of 0.5 ps). The density is $\sim$0.977 g/ml at 330 K. All runs described here cover a total of 97 ns.

Trajectory Analysis

To analyze the dimer simulations, we used the radii of gyration of the system (Rg), the hydrophobic core (Rg-core, using the side chains of Leu, Val, and the two Phe residues for each chain) and the C_α root-mean-square deviation (rmsd) from the lowest energy conformation obtained in simulation R1, except when mentioned otherwise. This antiparallel β sheet structure can be described by a 16 + k $\leftrightarrow$ 22 $-$ k β sheet registry (i.e., intermolecular H bonds between residues 16 + k and 22 $-$ k of the two chains, with k = 0, 2, 4, and 6, and the C=O...HN and NH..O=C bonds formed). A H bond is defined if it satisfies DSSP conditions (Kabsch and Sander, 1983): the distance between the carbonyl oxygen and amide hydrogen (O..H) is less than 2.5 Å and the angle NHO $> 150^\circ$. To follow the orientation of the chains, the scalar product (d12) between the end-to-end unit vectors of each chain was calculated: d12 = 1 indicates parallel, -1 antiparallel, and 0 perpendicular register. The percentage of secondary structure in each frame was determined using the DSSP program (Kabsch and Sander, 1983). We also used the less stringent conditions used by Klimov and Thirumalai as described in their experimental procedure: a conformation is a β strand (or α helix) if the ϕ and ψ of any two consecutive residues are in the appropriate Ramachandran regions and no two consecutive residues are in α-helix (β strand) (Klimov and Thirumalai, 2003). The figures were produced using the MOLMOL software (Koradi et al., 1996). All event numbers refer to accepted event numbers and the conformations of low energy are described by β sheet registries with k = 0, 2, 4, and 6.

Acknowledgments

Sébastien Santini is supported by the Natural Sciences and Engineering Research Council of Canada. The ART calculations were done on the computers of the Réseau québécois de calcul de haute performance and the MD simulations at IGS, Marseille. N.M. is a Cottrell Scholar of Research Corporation.

Received: January 22, 2004
Revised: April 27, 2004
Accepted: April 28, 2004
Published: July 13, 2004

References

Balbach, J., Ishii, Y., Antzutkin, O., Leapman, R., Rizzo, N., Dyda, F., Reed, J., and Tycko, R. (2000). Amyloid fibril formation by $A\beta_{16-22}$, a seven-residue fragment of the Alzheimer's β-amyloid peptide, and structural characterization by solid state NMR. Biochemistry *39*, 13748–13759.

Barkema, G., and Mousseau, N. (1996). Event-based relaxation of continuous disordered systems. Phys. Rev. Lett. *77*, 4358–4361.

Benzinger, T., Gregory, D., Burkoth, T., Miller-Auer, H., Lynn, D., Botto, R., and Meredith, S. (2000). Two-dimensional structure of β-amyloid(10–35) fibrils. Biochemistry *39*, 3491–3499.

Berendsen, H., van der Spoel, D., and van Drunen, R. (1995). GROMACS: a message-passing parallel molecular dynamics implementation. Comput. Phys. Comm. *91*, 43–56.

Bitan, G., Vollers, S., and Teplow, D. (2003). Elucidation of primary structure elements controlling early amyloid β-protein oligomerization. J. Biol. Chem. *278*, 34882–34889.

Broglia, R., Tiana, G., Pasquali, S., Roman, H., and Vigezzi, E. (1998). Folding and aggregation of designed proteins. Proc. Natl. Acad. Sci. USA *95*, 12930–12933.

Chiti, F., Webster, P., Taddei, N., Clark, A., Stefani, M., Ramponi, G., and Dobson, C. (1999). Designing conditions for in vitro formation of amyloid protofilaments and fibrils. Proc. Natl. Acad. Sci. USA *96*, 3590–3594.

Chowdhury, S., Zhang, W., Wu, C., Xiong, G., and Duan, Y. (2003). Breaking non-native hydrophobic clusters is the rate-limiting step in the folding of an alanine-based peptide. Biopolymers *68*, 63–75.

Derreumaux, P. (1999). From polypeptide sequences to structures using Monte Carlo simulations and an optimized potential. J. Chem. Phys. *111*, 2301–2310.

Derreumaux, P. (2000). Generating ensemble averages for small proteins from extended conformations by Monte Carlo simulations. Phys. Rev. Lett. *85*, 206–209.

Derreumaux, P., and Schlick, T. (1998). The loop opening/closing motion of the enzyme triosephosphate isomerase. Biophys. J. *74*, 72–81.

Dima, R., and Thirumalai, D. (2002). Exploring protein aggregation and self-propagation using lattice models: phase diagram and kinetics. Protein Sci. *11*, 1036–1049.

Ding, F., Dokholyan, N., Buldyrev, S.V., Stanley, H., and Shakhnovich, E. (2002). Molecular dynamics simulation of the SH3 domain aggregation suggests a generic amyloidogenesis mechanism. J. Mol. Biol. *324*, 851–857.

Fandrich, M., Forge, V., Buder, K., Kittler, M., Dobson, C., and Diekmann, S. (2003). Myoglobin forms amyloid fibrils by association of unfolded polypeptide segments. Proc. Natl. Acad. Sci. USA *100*, 15463–15468.

Fezoui, Y., and Teplow, D. (2002). Kinetic studies of amyloid β-protein fibril assembly. J. Biol. Chem. *277*, 36948–36954.

Forcellino, F., and Derreumaux, P. (2001). Computer simulations aimed at structure prediction of supersecondary motifs in proteins. Proteins *45*, 159–166.

Gsponer, J., Haberthur, U., and Caflisch, A. (2003). The role of side-chain interactions in the early steps of aggregation: molecular dynamics simulations of an amyloid-forming peptide from the yeast prion Sup35. Proc. Natl. Acad. Sci. USA *100*, 5154–5159.

Harrison, P., Chan, H., Prusiner, S., and Cohen, F. (2001). Conformational propagation with prion-like characteristics in a simple model of protein folding. Protein Sci. *10*, 819–835.

Ikeda, K., and Higo, J. (2003). Free-energy landscape of a chameleon sequence in explicit water and its inherent α/β bifacial property. Protein Sci. *12*, 2542–2548.

Istrail, S., Schwartz, R., and King, J. (1999). Lattice simulations of aggregation funnels for protein folding. J. Comput. Biol. *6*, 143–162.

Jang, H., Hall, C., and Zhou, Y. (2004). Assembly and kinetic folding pathways of a tetrameric β-sheet complex: molecular dynamics simulations on simplified off-lattice protein models. Biophys. J. *86*, 31–49.

Kabsch, W., and Sander, C. (1983). Dictionary of protein secondary structure: pattern recognition of hydrogen-bonded and geometrical features. Biopolymers *22*, 2577–2637.

Kelly, J. (1996). Alternative conformations of amyloidogenic proteins govern their behavior. Curr. Opin. Struct. Biol. *6*, 11–17.

Kirkitadze, M., Condron, M., and Teplow, D. (2001). Identification and characterization of key kinetic intermediates in Amyloid β-protein fibrillogenesis. J. Mol. Biol. *312*, 1103–1119.

Klimov, D., and Thirumalai, D. (2003). Dissecting the assembly of $A\beta_{16-22}$ amyloid peptides into antiparallel β-sheets. Structure (Camb) *11*, 295–307.

Koradi, R., Billeter, M., and Wüthrich, K. (1996). Molmol: a program for display and analysys of molecular structures. J. Mol. Graph. *14*, 51.

Lansbury, P.J., Costa, P., Griffiths, J., Simon, E., Auger, M., Halverson, K., Kocisko, D., Hendsch, Z., Ashburn, T., Spencer, R. et al. (1995). Structural model for the β-amyloid fibril based on interstrand alignment of an antiparallel-sheet comprising a C-terminal peptide. Nat. Struct. Biol. *2*, 990–998.

Ma, B., and Nussinov, R. (2002). Stabilities and conformations of Alzheimer's β-amyloid peptide oligomers ($a\beta_{16-22}$, $a\beta_{16-35}$, and $a\beta_{10-35}$): sequence effects. Proc. Natl. Acad. Sci. USA *99*, 14126–14131.

Massi, F., Klimov, D., Thirumalai, D., and Straub, J. (2002). Charge states rather than propensity for β-structure determine enhanced fibrillogenesis in wild-type Alzheimer's β-amyloid peptide compared to E22Q Dutch mutant. Protein Sci. *11*, 1639–1647.

Miravalle, L., Tokuda, T., Chiarle, R., Giaccone, G., Bugiani, O., Tagliavini, F., Frangione, B., and Ghiso, J. (2000). Substitutions at codon 22 of Alzheimer's Aβ peptide induce diverse conformational changes and apoptotic effects in human cerebral endothelial cells. J. Biol. Chem. *275*, 27110–27116.

Mousseau, N., Derreumaux, P., Barkema, G., and Malek, R. (2001). Sampling activated mechanisms in proteins with the activation-relaxation technique. J. Mol. Graph. Model. *19*, 78–86.

Petkova, A., Ishii, Y., Balbach, J., Antzutkin, O., Leapman, R., Delaglio, F., and Tycko, R. (2002). A structural model for Alzheimer's β-amyloid fibrils based on experimental constraints from solid state NMR. Proc. Natl. Acad. Sci. USA *99*, 16742–16747.

Petkova, A., Buntkowsky, G., Dyda, F., Leapman, R., Yau, W., and Tycko, R. (2004). Solid state NMR reveals a pH-dependent antiparallel β-sheet registry in fibrils formed by a β-amyloid peptide. J. Mol. Biol. *335*, 247–260.

Prusiner, S. (1997). Prion diseases and the BSE crisis. Science *278*, 245–251.

Santini, S., Wei, G., Mousseau, N., and Derreumaux, P. (2003). Exploring the folding pathways of proteins through energy landscape sampling: application to alzheimer's β-amyloid peptide. Internet Electron. J. Mol. Des. *2*, 564–577.

Selkoe, D. (1998). The cell biology of β-amyloid precursor protein and presenilin in Alzheimer's disease. Trends Cell Biol. *8*, 447–453.

Shao, H., Jao, S., Ma, K., and Zagorski, M. (1999). Solution structures of micelle-bound amyloid β-(1–40) and β-(1–42) peptides of Alzheimer's disease. J. Mol. Biol. *285*, 755–773.

Sikorski, P., Atkins, E., and Serpell, L. (2003). Structure and texture of fibrous crystals formed by Alzheimer's Aβ(11–25) peptide fragment. Structure *11*, 915–926.

Silow, M., Tan, Y., Fersht, A., and Oliveberg, M. (1999). Formation of short-lived protein aggregates directly from the coil in two-state folding. Biochemistry *38*, 13006–13012.

Silva, R., Barber-Armstrong, W., and Decatur, S. (2003). The organization and assembly of a β-sheet formed by a prion peptide in solution: an isotope-edited FTIR study. J. Am. Chem. Soc. *125*, 13674–13675.

Talafous, J., Marcinowski, K., Klopman, G., and Zagorski, M. (1994). Solution structure of residues 1–28 of the amyloid β-peptide. Biochemistry *33*, 7788–7796.

Tjernberg, L., Tjernberg, A., Bark, N., Shi, Y., Ruzsicska, B., Bu, Z., Thyberg, J., and Callaway, D. (2002). Assembling amyloid fibrils from designed structures containing a significant amyloid β-peptide fragment. Biochem. J. *366*, 343–351.

Walsh, D., Lomakin, A., Benedek, G., Condron, M., and Teplow, D. (1997). Amyloid β-protein fibrillogenesis. Detection of a protofibrillar. J. Biol. Chem. *272*, 22364–22372.

Walsh, D., Hartley, D., Kusumoto, Y., Fezoui, Y., Condron, M., Lomakin, A., Benedek, G., Selkoe, D., and Teplow, D. (1999). Amyloid β-protein fibrillogenesis. Structure and biological activity of protofibrillar intermediates. J. Biol. Chem. *274*, 25945–25952.

Walsh, D., Klyubin, I., Fadeeva, J., Cullen, W., Anwyl, R., Wolfe, M., and Rowan, M. (2002). Naturally secreted oligomers of amyloid β-protein potently inhibit hippocampal long-term potentiation in vivo. Nature *416*, 483–484.

Wei, G., Mousseau, N., and Derreumaux, P. (2002). Exploring the energy landscape of proteins: a characterization of the activation-relaxation technique. J. Chem. Phys. *117*, 11379–11387.

Wei, G., Derreumaux, P., and Mousseau, N. (2003). Sampling the complex energy landscape of a simple β-hairpin. J. Chem. Phys. *119*, 6403–6406.

Wolfe, M. (2002). Therapeutic strategies for Alzheimer's disease. Nat. Rev. Drug Discov. *1*, 859–866.

Zagorski, M., Shao, H., Ma, K., Yang, J., Li, H., Zhang, Y., and Papolla, M. (2000). Amyloid Aβ(1–40) and Aβ(1–42) adopt remarkably stable, monomeric, and extended structures in water solution at neutral pH. Neurobiol. Aging *21*, 10–11.

Zhang, S., Iwata, K., Lachenmann, M., Peng, J., Li, S., Stimson, E., Lu, Y., Felix, A., Maggio, J., and Lee, J. (2000). The Alzheimer's peptide Aβ adopts a collapsed coil structure in water. J. Struct. Biol. *130*, 130–141.